Journal of Solid State Chemistry 184 (2011) 1682–1687

Contents lists available at ScienceDirect

Journal of Solid State Chemistry

journal homepage: www.elsevier.com/locate/jssc

Effect of transition element doping on crystal structure of rare earth borosilicides $REB_{44}Si_2$

D. Berthebaud [a], A. Sato [a], Y. Michiue [a], T. Mori [a,*,1], A. Nomura [b], T. Shishido [b], K. Nakajima [b]

[a] National Institute for Materials Science (NIMS), Namiki 1-1, Tsukuba 305-0044, Japan
[b] Institute for Materials Research, Tohoku University, 2-1-1 Katahira, Aoba-ku, Sendai 980-8577, Japan

ARTICLE INFO

Article history:
Received 29 October 2010
Received in revised form
20 April 2011
Accepted 24 April 2011
Available online 8 May 2011

Keywords:
Borides
Crystals
Doping
Transition elements

ABSTRACT

On a previous study on samples of doped-$YB_{44}Si_2$, an improvement of thermoelectric properties has been achieved. Regarding the interesting effect of the doping of transition elements on the thermoelectric properties, a single crystal study has been carried out on Zn doped, Rh doped and Ni doped samples to assess how the transition element doping affects the crystal structure. Refinements were carried out based on the structural model solution of $YB_{44}Si_2$ reported in a previous study. Variations in the silicon contents were found in the doped single crystals. Splitting of partially occupied sites has also been detected for some of the doped samples. In this paper we present differences in the partial occupations of boron and silicon sites. Possibility of transition elements insertions based on the differences in crystal structures will be presented.

© 2011 Elsevier Inc. All rights reserved.

1. Introduction

Research in boron and borides has been a topic of longstanding interest [1,2]. Recently there have been several discoveries of striking phenomena in compounds containing boron, like the superconductivity in MgB_2 [3], strong magnetic coupling in magnetically dilute boride insulators [4–6], and new elemental form of boron [7], for example. The high temperature ferromagnetism reported in doped CaB_6 also attracted a lot of interest [8], but it was proved to be nonintrinsic, i.e. originate from iron impurities [9,10]. Thermoelectric properties of some compounds containing boron have also attracted some interest like higher boride compounds such as $REB_{22}C_2N$ (RE=rare earth) [11,12] and $REB_{44}Si_2$ [13], which are under investigation, since they are high-temperature materials and exhibit intrinsic low thermal conductivity, making them potentially good thermoelectric materials at high temperatures.

The notation $REB_{44}Si_2$ is used to avoid confusion between all these isostructural compounds with different chemical compositions such as $YB_{41}Si_{1.2}$ [14] and $TbB_{44}Si_{0.7}$ [15]. This difference is due to the fact that the $REB_{44}Si_2$ structure is characterized by a large number of Si and B sites with various partial occupancies, forming polyhedron $B_{12}Si_3$ and composing interstitial sites. This structure type has first been resolved by Higashi et al. [14] on a crystal of $YB_{41}Si_{1.2}$ grown by the floating-zone method.

In a larger scope, the boron cluster structures have been studied with great interest over the years for such compounds as borides [1,16–21] and boranes [22–24]. Boron-rich borides tend to have the boron icosahedra cluster B_{12} as the basic building block of the structure. The arrangement of the boron clusters forms the framework of the crystal structure [1,16–21]. In 1986, Higashi classified the B_{12} icosahedral compounds known at that time into 8 basic types: (1) α-rhombohedral boron type; (2) β-rhombohedral boron type; (3) α-tetragonal boron type; (4) β-tetragonal boron type; (5) AlB_{10} (or AlC_4B_{26}) type; (6) NaB_{15} type; (7) YB_{66} type; and (8) γ-AlB_{12} type [20]. The $REB_{44}Si_2$ structure represents a new type of structure. We note that among the metal-boron-silicon compounds other new compounds have also recently been reported such as $RE_{3-x}B_{36}Si_8C_2$ [25], $RE_{1-x}B_{12}Si_{3.3-d}$ [26] and $MgB_{12}Si_2$ [27]. Compared to $RE_{3-x}B_{36}Si_8C_2$ and $RE_{1-x}B_{12}Si_{3.3-d}$ and actually most of the rare earth higher borides [1], the structure of the $REB_{44}Si_2$ system is notable in that the rare earth site has full occupancy, and there is also a $B_{12}Si_3$ polyhedron in addition to the five structurally independent B_{12} icosahedral clusters. The rare earth sites have a ladder-like configuration, which together with the full occupancy is responsible for some of the interesting physical properties. $REB_{44}Si_2$ exhibits strong magnetic coupling despite being a magnetically dilute boride f-electron insulator, as mentioned above [4,15]. It has been shown to have a dimer-like antiferromagnetic transition with magnetic rare earth ions forming pairs along a one-dimensional chain parallel to the c-axis [28]. Large differences in the behavior of thermal conductivity compared with REB_{66} were also observed [29].

* Corresponding author.
E-mail address: MORI.Takao@nims.go.jp.(T. Mori)

0022-4596/$ - see front matter © 2011 Elsevier Inc. All rights reserved.
doi:10.1016/j.jssc.2011.04.038

In a previous study, transition metal doping in $REB_{44}Si_2$ has been investigated in order to improve thermoelectric properties [30]. Samples have been prepared by arc-melting with addition of transition elements (Mo, Mn, Fe, Rh, Ti, Cu, Zn, etc.) to synthesize doped-$YB_{44}Si_2$. Among the differently doped samples, it was found that Zn doping significantly improved the thermoelectric power factor of the borosilicide $YB_{44}Si_2$ by more than 30% [30]. Then as analyses showed that zinc did not remain in the final product but has an effect to improve crystal quality, further investigations were needed to make clear any doping effects on the crystal structure of borosilicides. Crystal structure studies of borosilicides doped with Zn, Rh and Ni are presented in this article.

2. Experimental section

As described in Ref. [18], polycrystalline samples were prepared by arc-melting of the appropriate amounts of powders of YB_4, B, Si and transition metals to form $YB_{44}Si_2$:*Tr* (*Tr*=transition metal). Samples were then preliminary characterized by powder X-ray diffraction (RIGAKU RINT-ULTIMA3). Small single crystals suitable for X-ray diffraction were isolated from each sample. X-ray single crystal diffraction data were collected using a Bruker Smart Apex CCD difractometer with Mo$K\alpha$ radiation. The program SMART-NT was used for data collection [31]. Cell refinement and data reduction were achieved with SAINT-PLUS-NT software [32]. An empirical absorption correction based on comparison of redundant and equivalent reflections was applied using SADABS [33]. The crystal structure solution was accomplished through the program SIR2004 [34]. The different structural parameters (atomic coordinates, thermal parameters and occupation statistics) were refined by the least-square method using atomic scattering factors provided by the program package SHELXL-97 [35]. Composition and microstructure were checked by an FEI Quanta FEG 200 scanning electron microscope (SEM) equipped with an Oxford INCA energy dispersive X-ray spectroscopy system (EDX).

3. Results and discussion

The first description by Higashi et al. [14] of the $YB_{44}Si_2$ structure prepared by the floating-zone method reported a structure characterized by a framework of five different B_{12} icosahedral and $B_{12}Si_3$ polyhedron (see Fig. 1) with an approximate composition of $YB_{41}Si_{1.2}$. The unit cell include fifty-three different boron crystallographic sites of which seven are partially occupied, two sites occupied by yttrium and silicon atoms, respectively, and three sites partially occupied by both silicon and boron. Single crystal study of our non-doped $YB_{44}Si_2$ sample prepared by arc-melting (crystal A) shows some minor structure differences from the one of the Higashi study. Refinement of the pure sample converged to a structural model with an atom distribution approximate to $YB_{41}Si_{1.2}$ and lattice parameters at ambient temperature $a=16.680(5)$, $b=17.652(5)$ and $c=9.512(5)$ Å. Refinements of anisotropic displacements have been carried out for yttrium, silicon and sites partially occupied by two atoms types resulting in low values of the residual factors. Lattice parameters of all samples doped and non-doped are reported in Table 1. The chemical composition and the $R(R_w)$ show similar values to the Higashi crystal. Unit cell includes fifty boron sites within three partially occupied sites, one yttrium site, one silicon site and three sites partially occupied by boron and silicon. Refinement has been carried out considering partial occupation by boron of the three Si sites of the $B_{12}Si_3$ polyhedron

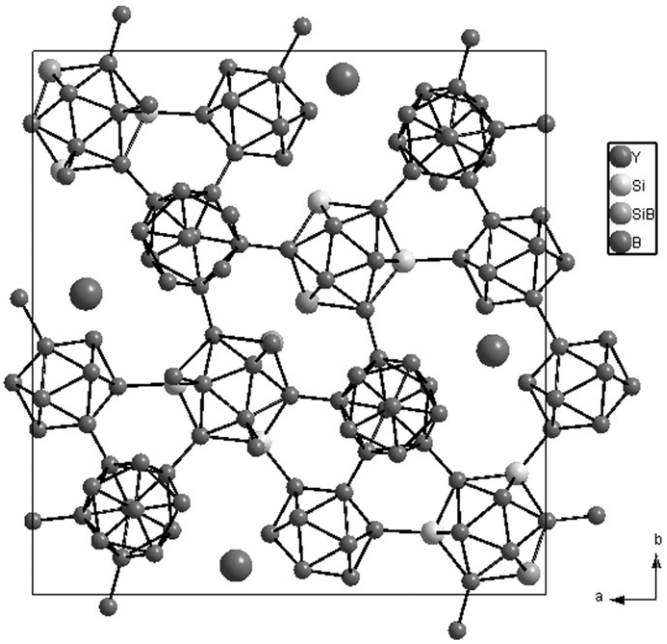

Fig. 1. View of the crystal structure of $YB_{44}Si_2$ along the *c*-axis. Arrangements of two kinds of polyhedral are shown: B_{12} icosahedra and $B_{12}Si_3$ polyhedra. Only two of the five structurally independent B_{12} icosahedra are drawn for clarity. Yttrium atoms are localized between the polyhedrons.

as in the previous study; we also notice that one of these sites was obviously occupied by both Si and B atoms because of the too short Si–Si distances making a simultaneous occupation by Si atoms impossible (~1.74 Å).

As has been discussed previously in the crystal growth study of $REB_{44}Si_2$ [36], different chemical compositions might be obtained for REB_{50}-type compounds due to the various partially occupied sites. Crystal growth method also plays a role, for example, silicon excess and/or growth speed rate are important parameters to control the final composition [36]. In our case, the differences between our crystal and the Higashi one probably can be attributed to difference in the crystal grown speed and in the crystal quality itself, as the one prepared by the floating-zone method might allow observation of low intensities of electronic densities such as the partially occupied boron sites with very low occupancies values. Therefore for the rest of this study, we have considered the non-doped $YB_{44}Si_2$ prepared by arc-melting as an initial model to compare any structural changes induced in transition elements doped samples prepared with similar conditions.

Next, single crystal study was carried out on the doped sample done with an addition of zinc (crystal B) as it was the one exhibiting the most interesting properties [30]. Its thermoelectric properties were improved but chemical analyses have shown that zinc did not remain in the final sample; however this addition to the synthesis appears to have an effect to improve the crystallinity of the sample [30]. A single crystal selected from this preparation was measured. Structure calculations were carried out with Y, B and Si atoms. In subsequent refinements, silicon contents have been evidenced to be higher than for the standard sample. Final refinements rapidly converged to low residual factors and yielded a featureless Fourier difference map. The final calculated chemical composition was approximate to $YB_{41.1}Si_{1.43}$. As already noticed in some previous studies [37,38] the increase of silicon content is characterized by a significant enlargement of lattice parameters, which increase to $a=16.708(5)$, $b=17.674(5)$ and $c=9.532(5)$ Å. The improvement of the thermoelectric properties pointed out in the previous study may be

Table 1
Crystal data and structure refinements of $YB_{41}Si_{1.2}$ (A), Zn added $YB_{41.1}Si_{1.43}$ (B), $YB_{41.1}Si_{1.1}Rh_{0.02}$ (C) and $YB_{41}Si_{1.3}Ni_{0.06}$ (D).

Crystal label	A	B	C	D
Empirical formula	$YB_{41}Si_{1.25}$	$YB_{41.2}Si_{1.42}$	$YB_{41.1}Si_{1.1}Rh_{0.02}$	$YB_{41}Si_{1.3}Ni_{0.06}$
Formula weight (g mol^{-1})	567.9	574.5	566.1	573.3
Crystal system, space group	*Pbam*			
Unit cell dimensions (Å)				
a	16.680(5)	16.708(5)	16.673(5)	16.702(5)
b	17.652(5)	17.674(5)	17.659(5)	17.666(5)
c	9.512(5)	9.532(5)	9.511(5)	9.522(5)
Volume (Å^3)	2800.67	2814.91	2800.31	2809.54
Z, Calculated density (g/cm^3)	8, 2.69	8, 2.71	8, 2.68	8, 2.71
R (int)	0.0355	0.042	0.052	0.044
Number of independent reflections	3117	3144	3150	3117
Refined parameters	224	224	231	231
Goodness-of-fit on F^2	1.131	1.084	1.105	1.164
WR_2	0.107	0.106	0.1207	0.1183
R_1 [$I > 2\sigma(I)$]	0.0358	0.036	0.0407	0.0469
The largest difference peak and hole (e Å^{-3})	2.63/−0.437	2.335/−0.518	2.169/−0.577	1.764/−0.679

$R(F) = \Sigma||F_o|-|F_c||/\Sigma|F_o|$, $WR_2 = [\Sigma W(F_0^2 - F_c^{2)2}/\Sigma WF_0^4]^{1/4}$, where $W^{-1} = [\sigma^2(F_0^2) + 7.27P]$, $P = [\max(F_0^2, 0) + 2F_c^2]/3$.

related to the presence of Zn in the starting composition, which plays a role to increase the silicon content by around 15%. In one scenario, zinc might react with a part of the boron from the initial composition and allow more silicon to be inserted in the structure during the melting reaction resulting in a better crystal quality. Outside the differences in partial occupancies values of boron-silicon sites no structural differences have been evidenced in this crystal. Lattice parameters, crystallographic data and refinements parameters for $YB_{41.1}Si_{1.43}$ are shown in Table 1.

Rh and Ni doped samples (respectively, crystals C and D) have also been studied by single crystal X-ray diffraction. In those cases, chemical analyses show that these elements remain in the final composition. X-ray powder diffraction patterns showed presence of impurities phases including Ni and Rh [30]. Crystal structure determinations have been carried out to investigate the possibility of the transition elements insertion in the structure of $YB_{44}Si_2$. Firstly, structure calculations were carried out considering only Y, B and Si atoms. Final refinements rapidly converged to low residual factors and yielded a featureless Fourier difference map. The final calculated chemical compositions were approximately $YB_{40.5}Si_{1.6}$ for the sample with Ni, and $YB_{40.8}Si_{1.25}$ for the sample with Rh. Lattice parameters were $a = 16.702(5)$, $b = 17.666(5)$ and $c = 9.522(5)$ Å for the sample with Ni and $a = 16.673(5)$, $b = 17.659(5)$ and $c = 9.511(5)$ Å for the sample with Rh. During the refinement, a residual electronic density indicated a new partially occupied position between B_{12} icosahedra. This position is partially occupied by a silicon atom. For both cases, the distance B–Si between this silicon atom and the two boron atoms on the apex of icosahedra is too short (less than 1 Å) to allow a simultaneous occupation by boron and silicon, thereby indicating splitting positions. Mixed occupancy of split positions has already been observed for higher borides compounds such as for incorporation of carbon in quaternary *RE*–B–C–Si compounds [39]. Fig. 2 shows B_{12} icosahedra with insertion of silicon between two of them; boron atoms in position 8*i* and silicon atom in position 4*h* are shown although simultaneous occupation is not possible. Fig. 3(a) shows how the bonding scheme is transformed when the position between icosahedra is occupied by a silicon atom. Two boron atoms are removed and the icosahedra turn into B_{11} polyhedrons, which is an unusual configuration in the case of inorganic compounds but which has been already observed for transition metals organometallics compounds. Boron atom polyhedron have been found in the *closo*-hydroborates $[B_nH_n]^{2-}$ with $n = 5$–12 [24]. Fig. 3(b) shows regular B_{12} icosahedra chains in case of boron partial occupancy. Such icosahedra in boron-rich

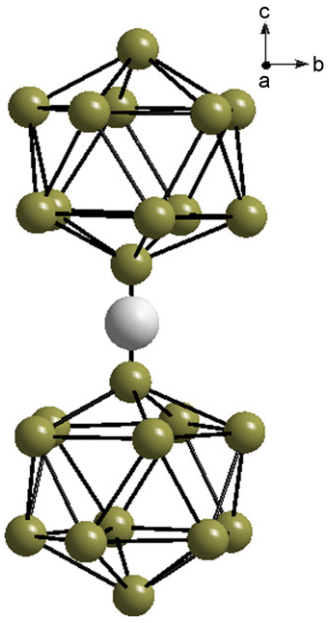

Fig. 2. B_{12} icosahedra with silicon or transition element split positions simultaneously shown.

solids are known to exhibit high concentrations of well-defined intrinsic structural defects. Some of those defects manifest as missing or incomplete occupation of some atomic positions; such partially occupied sites can be considered as possible insertion sites for doping. The estimated chemical compositions obtained from structure analysis revealed high silicon contents that are not consistent with the lattice parameters values as increase of silicon content is usually characterized by an increase of the lattice volume (as discussed above). Considering the possibility of the insertion of transitions elements, structure calculations were carried out with Y, B, Si and *Tr* (Rh and Ni). Transition metals were assigned on the position 4*h* between B_{12} icosahedra instead of a silicon atom. In subsequent refinements the occupancies on 4*h* and 8*i* sites were allowed to vary but total occupations (4*h*+8*i*) were constrained to one, yielding partial occupation of 0.12 and 0.04 of 4*h* sites, respectively, for Ni and Rh doping. Final refinements converged to low residual factors and yielded a featureless Fourier difference map. The initial model showed peaks in the Fourier difference maps. These were initially

assigned to partially occupied Si, but were eventually identified as the impurity transition metal atoms. The final calculated chemical compositions were approximately $YB_{41.1}Si_{1.1}Rh_{0.02}$ for the sample with Rh, and $YB_{41}Si_{1.3}Ni_{0.06}$ for the sample with Ni. After assuming insertion of transition metals the new estimated chemical composition gave silicon content in agreement with the lattice parameters, which in addition to structural change makes highly probable the transition elements insertion between B_{12} icosahedra instead of silicon atoms as suggested for the first time. Selected maps of the electron density around the partially occupied positions are shown in Fig. 4. Selected interatomic distances for $YB_{41.1}Si_{1.1}Rh_{0.02}$ and $YB_{41}Si_{1.3}Ni_{0.06}$ are shown in Table 3. The atomic radii sums for Rh–B and Ni–B are, respectively, 2.25 and 2.14 Å. In the case of rhodium insertion some distances appear to be shorter than this sum (Table 3); however this not unusual for borides, especially for rhodium borides compounds where distances shorter than 2 Å have been reported previously [40]. For nickel insertion, distances agree with previously reported crystal structures such as Ni_3B [41] and with the atomic radii sum. In order to get additional evidence that transition elements were inserted into the structure, EDX analyses were performed on doped samples. EDX results were in agreement with single crystal structure refinements results. Lattice parameters, crystallographic data and refinements parameters for $YB_{41.1}Si_{1.1}Rh_{0.02}$ and $YB_{41}Si_{1.3}Ni_{0.06}$ are shown in Table 1. Structure data details for $YB_{41.1}Si_{1.1}Rh_{0.02}$ are given in Table 2.

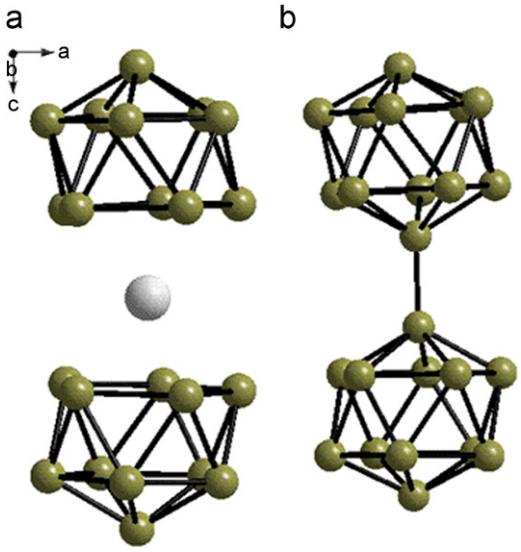

Fig. 3. Bonding scheme in each case of split position (a) partial occupancy by a silicon or transition element atom, surrounded by B_{11} polyhedron (b) B_{12} icosahedral chains.

In terms of the physical properties previously observed in the doped samples [30], the present structural analysis sheds a little more light. Our structural analysis indicates that a small amount of intrinsic doping of the transition metal atoms Ni and Rh into

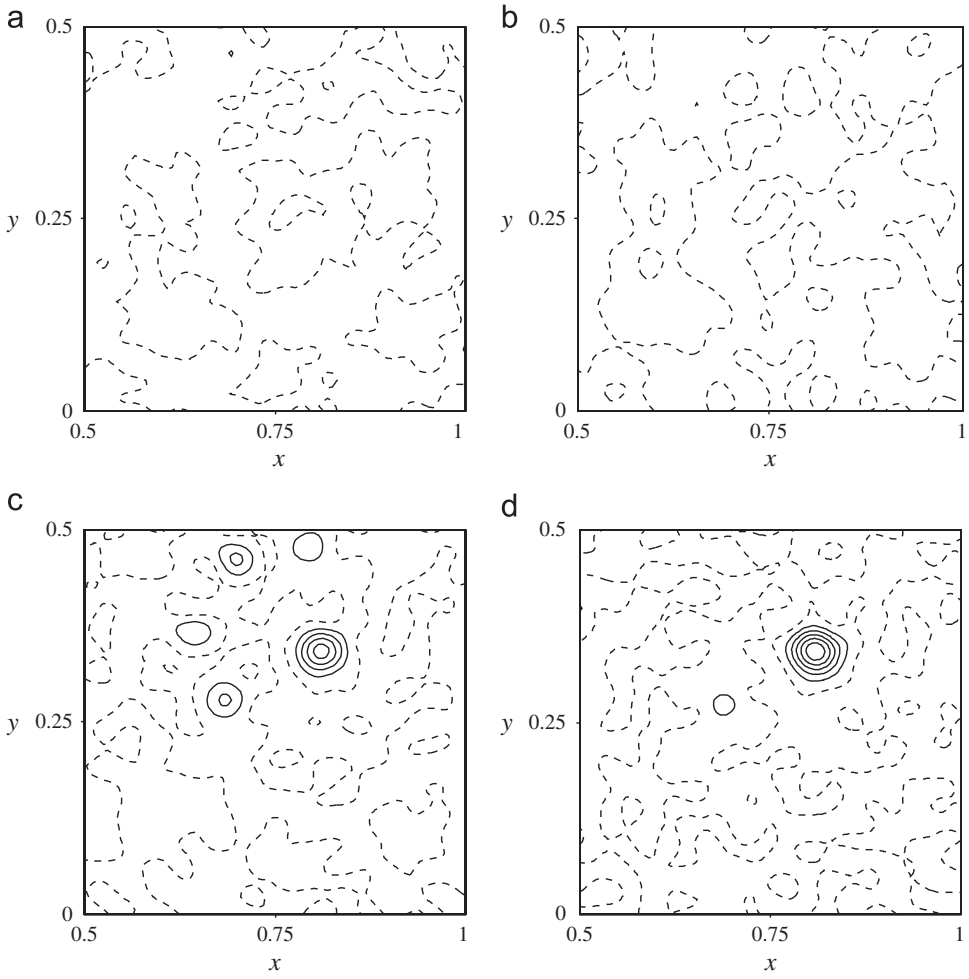

Fig. 4. Difference electron density maps in the vicinity of the assumed transition elements atom position (a) Residual electron densities at $z=0.5$ for sample A. (b) Residual electron densities at $z=0.5$ for sample B. (c) Residual electron densities at $z=0.5$ for sample C. No atoms are assumed between the B_{12} icosahedra. (d) Residual electron densities at $z=0.5$ for sample D. No atoms are assumed between the B_{12} icosahedra. Contour intervals are 1 e/Å^3. Broken lines are zero levels.

Table 2
$YB_{41.1}Si_{1.1}Rh_{0.02}$ atomic coordinates (x, y, z), isotropic (U_{iso}) or equivalent isotropic (U_{eq}) displacement parameters, their estimated standard deviations and occupancies.

Atom	Site	x	y	z	U_{iso}/U_{eq} (Å^2)	Occupancy
Y1	8*i*	0.1037(5)	0.0520(1)	0.2295(5)	0.0071(2)	1.0
Si1	4*h*	0.5569(2)	0.2211(4)	1/2	0.0114(3)	0.49(1)
Si2	4*h*	0.2216(8)	0.3867(5)	−1/2	0.0089(7)	0.53(1)
Si3	4*h*	0.1561(2)	0.0800(1)	1/2	0.0076(5)	0.74(1)
Si4	4*h*	0.0346(2)	0.4625(2)	1/2	0.0146(1)	0.45(1)
B1	4*h*	0.5569(2)	0.2211(4)	1/2	0.0114(3)	0.51(1)
B2	4*h*	0.2216(8)	0.3867(5)	−1/2	0.0089(7)	0.47
B3	4*h*	0.0346(2)	0.4625(2)	1/2	0.0146(1)	0.55
B4	4*g*	0.1381(5)	−0.0307(4)	0	0.0062(2)	1.0
B5	4*g*	0.0498(4)	0.1253(4)	0	0.0043(2)	1.0
B6	8*i*	−0.0973(5)	0.3557(2)	0.3316(5)	0.0062(1)	1.0
B7	8*i*	−0.1070(4)	0.1875(7)	0.4056(2)	0.0068(9)	1.0
B8	8*i*	−0.2606(4)	0.2781(3)	0.3353(1)	0.0069(2)	1.0
B9	8*i*	0.0637(2)	0.5488(9)	−0.0937(7)	0.0059(7)	1.0
B10	4*g*	0.0940(3)	0.4711(9)	0	0.0073(1)	1.0
B11	4*h*	0.1207(5)	−0.0324(4)	1/2	0.0077(7)	1.0
B12	4*g*	0.1896(5)	0.4450(4)	0	0.0055(2)	1.0
B13	8*i*	−0.0355(1)	0.2576(8)	−0.0947(8)	0.0064(9)	1.0
B14	8*i*	0.1208(1)	0.1881(3)	0.0972(6)	0.0063(1)	1.0
B15	8*i*	0.2989(7)	0.1542(4)	0.0883(1)	0.0056(5)	1.0
B16	8*i*	−0.0176(1)	0.1411(5)	0.3361(4)	0.0066(9)	1.0
B17	8*i*	0.0340(9)	0.4613(5)	−0.1566(5)	0.0056(1)	1.0
B18	4*g*	0.0320(6)	0.3144(6)	0	0.0054(5)	1.0
B19	8*i*	0.2625(7)	0.0745(3)	0.1814(8)	0.0056(1)	1.0
B20	4*h*	0.0376(8)	0.1119(1)	1/2	0.0085(3)	1.0
B21	8*i*	−0.1507(8)	0.2623(7)	0.3306(6)	0.0066(9)	1.0
B22	8*i*	0.1150(9)	−0.0922(6)	0.3351(7)	0.0065(3)	1.0
B23	8*i*	−0.0015(6)	0.3655(5)	0.4042(4)	0.0078(5)	1.0
B24	8*i*	0.1666(6)	−0.0852(1)	0.1632(8)	0.0059(3)	1.0
B25	8*i*	0.2090(6)	0.1677(5)	0.1833(1)	0.0063(4)	1.0
B26	8*i*	0.0647(5)	0.2693(7)	−0.1582(2)	0.0061(8)	1.0
B27	4*g*	−0.0422(5)	0.1721(6)	0	0.0055(5)	1.0
B28	8*i*	0.3259(1)	0.0677(7)	0.3371(1)	0.0081(3)	1.0
B29	8*i*	0.0257(7)	−0.0448(7)	0.4063(1)	0.0076(1)	1.0
B30	8*i*	0.2106(6)	−0.1718(9)	0.0951(7)	0.0060(3)	1.0
B31	4*g*	0.1270(8)	0.2756(2)	0	0.0060(3)	1.0
B32	8*i*	0.3839(7)	0.1964(3)	0.1744(1)	0.0068(1)	1.0
B33	8*i*	0.070(1)	0.4212(5)	−0.3064(2)	0.0071(4)	1.0
B34	8*i*	0.0176(9)	0.1773(9)	0.1635(7)	0.0063(9)	1.0
B35	8*i*	0.2280(1)	0.1170(5)	0.3446(3)	0.0060(9)	1.0
B36	4*g*	0.1294(3)	−0.1294(3)	0	0.0063(6)	1.0
B37	8*i*	0.1684(4)	0.3859(7)	−0.3059(8)	0.0073(7)	1.0
B38	8*i*	0.2892(1)	0.2416(7)	0.1758(5)	0.0069(5)	1.0
B39	8*i*	0.0850(6)	0.3225(5)	−0.3053(2)	0.0073(7)	1.0
B40	8*i*	0.2326(4)	−0.0094(8)	0.0974(1)	0.0069(5)	1.0
B41	4*g*	0.2025(7)	0.3459(4)	0	0.0072(1)	1.0
B42	8*i*	0.3684(9)	0.0974(7)	0.1782(4)	0.0062(4)	1.0
B43	8*i*	0.2742(6)	−0.0997(0)	0.1586(2)	0.0056(6)	1.0
B44	8*i*	−0.1880(8)	0.3402(9)	0.5852(7)	0.0065(2)	0.96(1)
B45	8*i*	−0.3271(6)	0.2069(3)	0.4061(5)	0.0114(9)	1.0
B46	4*g*	0.0144(8)	0.4080(1)	0	0.0061(2)	1.0
B47	4*h*	−0.0118(5)	0.1977(6)	1/2	0.0089(1)	1.0
B48	4*g*	0.0432(9)	0.0214(9)	0	0.0064(3)	1.0
B49	8*i*	0.3534(2)	−0.0252(1)	0.4067(8)	0.0098(4)	1.0
B50	4*h*	0.1682(2)	−0.1187(3)	1/2	0.0095(1)	1.0
B51	4*g*	−0.0793(1)	0.3462(5)	0	0.0260(5)	0.67(3)
B52	8*i*	0.1086(5)	0.3756(8)	−0.1174(9)	0.0111(7)	0.40(3)
B53	4*g*	0.1458(9)	−0.2512(5)	0	0.0389(30	0.41(3)
Rh1	4*h*	−0.1898(7)	0.3406(6)	1/2	0.0129(4)	0.04(1)

Table 3
Selected interatomic distances (d, Å) in $YB_{41.1}Si_{1.1}Rh_{0.02}$ (C) and $YB_{41}Si_{1.3}Ni_{0.06}$ (D).

$YB_{41.1}Si_{1.1}Rh_{0.02}$		$YB_{41}Si_{1.3}Ni_{0.06}$	
Atom	d (Å)	Atom	d (Å)
Y1–B48	2.4645	Y1–B48	2.4622
B1|Si1–B47	1.8341	B1|Si1–B47	1.8458
B1|Si1–B23	2.0299	B1|Si1–B23	2.0377
B1|Si1–B39	2.0602	B1|Si1–B39	2.0702
B1|Si1–B45	2.1442	B1|Si1–B45	2.1265
B2|Si2–B50	1.8384	B2|Si2–B50	1.8715
B2|Si2–B37	2.0480	B2|Si2–B37	2.0637
B2|Si2–B45	2.0491	B2|Si2–B45	2.0870
B2|Si2–B49	2.1838	B2|Si2–B49	2.1839
Si3–B35	2.0116	Si3–B35	2.0154
Si3–B20	2.0539	Si3–B20	2.0590
Si3–B11	2.0703	Si3–B11	2.0604
B3|Si4–B3|Si4	1.7546	B3|Si4–B3|Si4	1.7433
B3|Si4–B23	2.0329	B3|Si4–B23	2.0337
B3|Si4–B33	2.0669	B3|Si4–B33	2.0779
B3|Si4-B49	2.0783	B3|Si4-B49	2.0959
Rh1–B35	2.1479	Ni1–B35	2.1458
Rh1–B21	2.2203	Ni1–B21	2.2256
Rh1–B6	2.2392	Ni1–B6	2.2273
Rh1–B8	2.2506	Ni1–B8	2.2476
Rh1–B28	2.2540	Ni1–B28	2.2551

the $YB_{44}Si_2$ crystal structure occurred. The Rh doped sample strikingly exhibited n-type characteristics [30] and this can now be surmised to occur from intrinsic doping of Rh. The zinc doped sample previously showed an interesting effect where, despite zinc not remaining in the sample, the crystallinity was considerably improved, thereby leading to a significant decrease of the electrical resistivity and improvement of thermoelectric properties [30]. However, the Seebeck coefficients also showed a small change that cannot normally be attributed to crystallinity changes. With the present structural analysis, it is indicated that there is an increase of silicon in the zinc doped compound, which can be causing such a change in the Seebeck coefficient due to intrinsic doping.

4. Conclusion

Crystal structure of transition metal doped borosilicides $YB_{44}Si_2$:Tr was refined. Structural changes were evidenced during this investigation. Zinc doping appears to increase the silicon content in the final structure even if zinc itself did not remain in the sample. This led to a larger volume cell compared to a non-doped sample. And we conjecture that one scenario of the origin of the improvement of the crystal quality achieved by zinc addition (leading to better thermoelectric properties) is that during the synthesis zinc might react with a part of the boron from the initial composition and allow more silicon to be inserted in the structure during the melting reaction resulting in a better crystal quality. Samples doped with rhodium and nickel were found to show some structural change through X-ray single crystal diffraction, and it is indicated that transition elements may have been inserted on a 4*h* site between chains of B_{12} icosahedra. Small quantities of inserted transition elements lead to the transformation of B_{12} icosahedra into B_{11} polyhedrons for a few percent of them. It appears that new transition elements doped $YB_{44}Si_2$ are synthesized and have nominal compositions $YB_{41.1}Si_{1.1}Rh_{0.02}$ and $YB_{41}Si_{1.3}Ni_{0.06}$. The intrinsic doping of silicon and rhodium into the zinc and rhodium doped samples, respectively, can be the origin of interesting physical properties previously observed.

Acknowledgment

This work was partly supported by grants from the Thermal & Electric Energy Technology Foundation, AOARD (AOARD 104144), and the Scientific Research on Priority Areas of New Materials Science Using Regulated Nano Spaces, the Ministry of Education, Science, Sports and Culture, Grant-in-Aid.

Appendix A. Supporting information

Supplementary data associated with this article can be found in the online version at doi:10.1016/j.jssc.2011.04.038. The ICSD numbers are 422970, 422971, 422972, 422973 for the non-doped, Zn doped, Rh doped, and Ni doped crystal structures, respectively.

References

[1] T. Mori, Higher Borides, in: K.A. Gschneidner Jr., J.-C. Bunzli, V. Pecharsky (Eds.), Handbook on the Physics and Chemistry of Rare Earths, vol. 38, North-Holland, Amsterdam, 2008, pp. 105–173.
[2] T.H. Geballe, B.T. Matthias, K. Andres, J.P. Maita, A.S. Cooper, E. Corenzwit, Science 160 (1968) 1443.
[3] J. Nagamatsu, N. Nakagawa, T. Muranaka, Y. Zenitani, J. Akimitsu, Nature 410 (2001) 63.
[4] T. Mori, T. Tanaka, J. Phys. Soc. Jpn. 68 (1999) 2033.
[5] T. Mori, A. Leithe-Jasper, Phys. Rev. B 66 (2002) 214419.
[6] T. Mori, H. Mamiya, Phys. Rev. B 68 (2003) 214422.
[7] A.R. Oganov, J. Chen, C. Gatti, Y. Ma, Y. Ma, C.W. Glass, Z. Liu, T. Yu, O.O. Kurakevych, V.L. Solozhenko, Nature 457 (2009) 863.
[8] D.P. Young, D. Hall, M.E. Torelli, Z. Fisk, J.L. Sarrao, J.D. Thompson, H.R. Ott, S.B. Oseroff, R.G. Goodrich, R. Zysler, Nature 397 (1999) 412.
[9] T. Mori, S. Otani, Solid State Commun. 123 (2002) 287.
[10] T. Mori, S. Otani, J. Phys. Soc. Jpn. 71 (2002) 1789.
[11] T. Mori, T. Nishimura, J. Solid State Chem. 179 (2006) 2908.
[12] T. Mori, T. Nishimura, K. Yamaura, E. Takayama-Muromachi, J. Appl. Phys. 101 (2007) 093714.
[13] T. Mori, J. Appl. Phys. 97 (2005) 093703.
[14] I. Higashi, T. Tanaka, K. Kobayashi, Y. Ishizawa, M. Takami, J. Solid State Chem. 133 (1997) 11.
[15] T. Mori, T. Tanaka, IEEE Trans. Mag. 37 (2001) 2144.
[16] V.I. Matkovich, R.F. Griese, J. Economy, Z. Kristallogr. 122 (1965) 116.
[17] J.L. Hoard, R.E. Hughes, in: E.L. Muetterties (Ed.), The Chemistry of Boron and its Compounds, Wiley, New York, 1967, p. 25.
[18] R. Naslain, A. Guette, P. Hagenmuller, J. Less Common Met. 47 (1976) 1.
[19] V.I. Matkovich and J. Economy, in: Boron and Refractory Borides, p.78, Springer–Heidelberg, Berlin, New York, 1977.
[20] I. Higashi, AIP Conf. Proc. 140 (1986) 1.
[21] P. Rogl, in: G. Effenberg (Ed.), Phase Diagrams of Ternary Metal–Boron–Carbon Systems, ASM International, Ohio, 1998.
[22] K.P. Callahan, M.F. Hawthorne, Adv. Organomet. Chem. 14 (C) (1976) 145–186.
[23] T.P. Fehlner, J.-F. Halet, J.-Y. Saillard, Molecular Clusters: A Bridge to Solid-State Chemistry, Cambridge University Press, Cambridge, 2007.
[24] L. Barton, Top. Curr. Chem. 100 (1982) 169.
[25] J.R. Salvador, D. Bilc, S.D. Mahanti, M.G. Kanatzidis, Angew. Chem. Int. Ed. Engl. 41 (2002) 844–846.
[26] F.X. Zhang, F.F. Xu, T. Mori, Q.L. Liu, T. Tanaka, J. Solid State Chem. 170 (2003) 75–81.
[27] T. Ludwig, H. Hillebrecht, J. Solid State Chem. 179 (2006) 1623–1629.
[28] T. Mori, J. Appl. Phys. 95 (2004) 7204.
[29] T. Mori, J. Martin, G. Nolas, J. Appl. Phys. 102 (2007) 073510.
[30] T. Mori, D. Berthebaud, T. Nishimura, A. Nomura, T. Shishido, K. Nakajima, Dalton Trans. 4 (39) (2010) 1027–1030.
[31] Bruker, SMART-NT. Version 5.625, Bruker AXS Inc., Madison, Wisconsin, USA, 1999.
[32] Bruker, SAINT-plus-NT. Version 6.45, Bruker AXS Inc., Madison, Wisconsin, USA, 1999.
[33] Bruker, SADABS Version 2.03, Bruker AXS Inc., Madison, Wisconsin, USA, 1999.
[34] M.C. Burla, M. Camalli, B. Carrozzini, G.L. Cascarano, C. Giacovazzo, G. Polidori, R. Spagna, J. Appl. Cryst. 36 (2003) 1103.
[35] G.M. Sheldrick, SHELXS97 and SHELXL97, Program for Structure Solution and Refinement, University of Göttingen, Germany, 1997.
[36] T. Mori, Z. Kristallogr. 221 (2006) 464.
[37] T. Mori, T. Tanaka, J. Alloys Compd. 288 (1999) 32.
[38] T. Mori, T. Tanaka, J. Phys. Soc. Jpn. 69 (2000) 579.
[39] T. Tanaka, A. Sato, F. Zhang, J. Phys.: Conf. Series (2009) 176.
[40] P. Salamakha, O. Sologub, C. Rizzoli, A.P. Gonçalves, M. Almeida, J. Solid State Chem. 177 (2004) 4237.
[41] S. Rundqvist, Acta Chem. Scand. 12 (4) (1958) 658.